The diffusion of dichloroethane in phase-segregated polyurethanes

Ta-min Feng*, William J. MacKnight and Nathaniel S. Schneider†
Department of Polymer Science and Engineering, University of Massachusetts, Amherst, MA 01003, USA
(Received 8 February 1990; revised 25 April 1990; accepted 17 May 1990)

The sorption and diffusion of 1,2-dichloroethane (DCE) has been studied in a series of polyurethanes based on diphenylmethane diisocyanate and butanediol with 1000 and 2000 molecular-weight poly(tetramethylene oxide) (PTMO). DCE is a strongly swelling solvent with solubilities as large as 450% in the commercial Estane sample (63% soft segment). The sorption isotherms for the Estane sample, determined on sorption and desorption cycles and for three sample thicknesses, coincide. Hysteresis is seen in the sorption isotherms of other samples with lower soft-segment content, the isotherm on desorption being higher than that on sorption. The sorption rate curves are generally Fickian at low concentrations but become sigmoidal at higher concentrations for sorption and desorption in the Estane and the PTMO-2000 sample with the highest soft-segment content (68%). For other samples the curves are two-stage for sorption but Fickian for desorption. Diffusion coefficients (D) were calculated by application of the analysis of coupled Fickian diffusion and first-order relaxation due to Joshi and Astarita. The resulting D *versus* C curves showed a maximum, attributable to the competing contributions of the solvent mobility and the thermodynamic factor. In addition, it was found that a correction to D for heating effects was required. There was evidence of significant solvent-induced structural relaxation in the higher hard-segment samples leading to higher than expected solubilities and diffusion constants. A pronounced thickness dependence of the diffusion constant could not be explained in terms of current diffusion models.

(Keywords: diffusion; dichloroethane; polyurethanes)

INTRODUCTION

The thermal transition behaviour, mechanical and structural properties of segmented polyurethanes based on diphenylmethane diisocyanate (MDI), butanediol (BD) and poly(tetramethylene oxide) (PTMO), or other polyethers, have been the subject of extensive study during the past decade[1–7]. As a result of the more recent studies of small-scale structure[8,9], and particularly the work of Koberstein *et al.* on the large-scale structural organization[10,11], a model has been developed that explains many of the key observations. According to this model, shorter hard-segment units, below a critical length, are mixed with the soft-segment phase. The interfacial region is diffuse due to the spatial requirements and irregularities in the chain folding of the MDI–BD hard-segment units. Organization in the hard-segment units is strongly dependent on the repeat-unit length and the thermal history. All of these features play a role in determining the mechanical properties of the sample and must also affect the interaction with solvents.

It is to be expected that solvents that not only swell the soft-segment phase but can interact with the hard-segment structure will lead to complex sorption behaviour. In a recent investigation, Schneider *et al.*[12] reported on vapour sorption studies with a strongly swelling liquid, *o*-dichlorobenzene (ODBZ), in an Estane sample, a commercial poly(tetramethylene oxide)-based polyurethane. At moderate to high concentrations, two-stage sorption behaviour occurred but was generally absent in desorption runs. The sorption curves could be fitted with the Berens–Hopfenberg model[13] of independent Fickian diffusion and relaxation processes. A maximum in the concentration dependence of the diffusion coefficient could be explained largely by the thermodynamic corrections that were applied to calculate the solvent mobility, D_1. Since D_1 did not show the expected strong increase with concentration, the authors suggested that relaxation processes also affected D_1. The presence of relaxation effects was attributed to coupling between the hard- and soft-segment phases, so that swelling in the soft-segment phase was controlled by solvent-induced hard-segment relaxation.

The behaviour studied by these authors was complicated by the need to make corrections for the pressure drift during their experiments, due to the low vapour pressure of ODBZ (1.4 mmHg/25°C). The present work was undertaken to clarify the observations made in the study with ODBZ by examining the influence of polyurethane composition on the anomalous diffusion behaviour and by using a high-vapour-pressure liquid, 1,2-dichloroethane. Thermal and mechanical characterization was also carried out on the samples and is reported.

EXPERIMENTAL

Samples

The polyurethane samples used in this study consisted of the Estane sample (Goodrich) reported on

* Current address: Union Carbide, PO Box 670/Building 98, Bound Brook, NJ 08805, USA
† To whom correspondence should be addressed at Polymer Research Branch, SLCMT-EMP, Army Materials Technology Laboratory, Watertown, MA 02172, USA

0032-3861/91/081493-11

earlier and a set of polyurethanes with varying hard-segment content, also based on diphenylmethane 4,4'-diisocyanate (MDI), butanediol (BD) and poly(tetramethylene oxide) (PTMO) of two molecular weights (PTMO-1000 and PTMO-2000). The samples were synthesized by a standard two-step procedure involving the initial end-capping of the PTMO with the required amount of MDI followed by chain extension with BD. Details are similar to the earlier published procedure[5]. The polyurethane samples are summarized in *Table 1*, where the designation PU2S44, etc., indicates a sample containing 44% by weight of PTMO-2000. Film samples were prepared by casting from a dimethylformamide (DMF) solution on an optically flat glass surface, which formed the base of a desiccator-like vessel. After the samples had been brought to dryness at room temperature under vacuum, the films were freed from the casting surface and transferred to a vacuum oven at 80°C for two days to complete solvent removal. The samples were then stored in a desiccator at room temperature.

Differential scanning calorimetry

D.s.c. thermograms over the temperature range from −110°C to about 230°C were recorded on a Perkin–Elmer DSC-7, interfaced with a thermal analysis data station. Calibration was done using indium and cyclohexane as standards. The experiments were carried out at a heating rate of 20°C min^{-1} under a helium purge. Two samples, APU1S44 and APU2S34, were annealed at 155°C for two days before conducting d.s.c. runs.

Tensile testing

Uniaxial stress–strain measurements were made at room temperature using an Instron 4202 tensile testing machine with a crosshead speed of 10 mm min^{-1}. The instrument was controlled by an HP computer, which automatically carries out the data analysis.

Vapour sorption measurements

Incremental vapour sorption and desorption measurements were carried out in a vacuum system contained within a thermostatted cabinet. Weight changes in the sample exposed to vapour were determined using a quartz spring enclosed in a water-jacketed sample chamber maintained at 24°C. The displacement of the spring was measured to 0.01 mm using a Gaertner cathetometer. The sample dimensions were approximately $2 \times 2\ cm^2$ to avoid errors due to edge effects. Pressure drifts during the run, such as those encountered with *o*-dichlorobenzene (ODBZ), were minimized in the present work by the use of 1,2-dichloroethane (DCE), which has a vapour pressure $p_0 = 74.8$ mmHg at 24°C. In addition, an increased ballast volume, consisting of both 5 litre and 15 litre spherical flasks, contributed to the pressure stability.

The measurements involved equilibrating the films with solvent at some vapour activity p_i/p_0, exposing the film to a step change in activity p_f/p_0, and recording the weight change as a function of time until equilibrium was achieved. This procedure was repeated in activity increments of about 0.1, up to an activity of about 0.8, beyond which much smaller increments were used. Owing to long-term changes in sample weight, many determinations required one day or more to attain equilibrium. After completing the set of sorption measurements, the procedure was reversed and desorption experiments were performed beginning with the film equilibrated at high activity. Once again, the full activity range was traversed by exposing the film to a step decrease in activity and recording the weight loss as a function of time.

RESULTS AND DISCUSSION

D.s.c. results

The combined set of d.s.c. scans for the various samples over the temperature range from −90 to 20°C, representing the region of the soft-segment glass transition temperature, appear in *Figure 1a* and the scans over the temperature range from 70 to 225°C, representing the region of the hard-segment transitions, appear in *Figure 1b*. The transition temperatures and the other thermal data are summarized in *Table 1*. The soft-segment glass transition temperature T_g is an indication of the phase mixing of hard-segment units with the soft-segment phase[14], whereas the magnitude of the heat capacity change at T_g can be used to obtain a measure of the soft segment incorporated in hard-segment domains[15]. The T_g of the three PTMO-1000 samples (*Figure 1a*) remains at about −40°C, independent of the hard-segment content. The invariant T_g, in this case, is not to be interpreted as an indication of strong phase separation

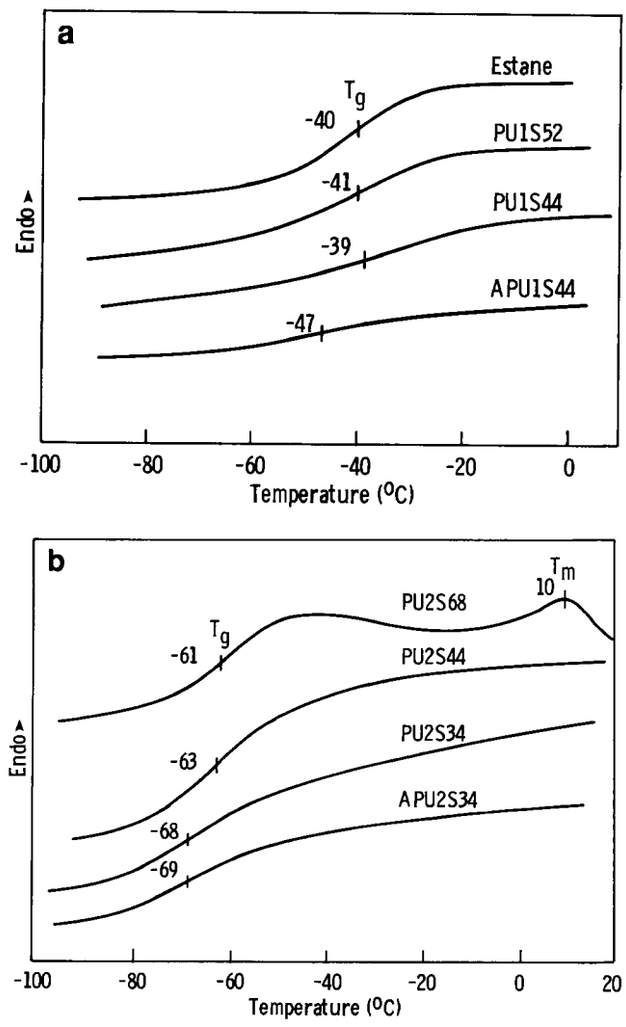

Figure 1 D.s.c. scans over the low-temperature range

Table 1 D.s.c. results on polyurethane samples

Sample	Mole ratio MDI/BD/PTMO	T_g (°C) of SS	Fraction of free SS	T_g (°C) of HS	T_m (°C) of HS	H (J g^{-1})[a] of HS	Crystalline percentage of HS
Estane	2/1/1	−40	0.48	95	152	5.9	4.5
PU1S52	3/2/1	−41	0.33	103	180	8.3	7.4
PU1S44	4/3/1	−39	0.25	104	184	21.4	19.0
APU1S44		−47	0.27		196	43.2	38.3
PU2S68	3/2/1	−61	0.58	112	179, 202	4.4	3.9
PU2S44	8/7/1	−63	0.39	115	189, 202	28.9	25.6
PU2S34	12/11/1	−68	0.27		193, 206	34.5	39.8
APU2S34		−69	0.31		194, 208	49.1	56.7
PTMO-2000		−79					
MDI-BD					192, 213	52.0	60.0

[a]Values normalized to weight fraction of hard segment

since the T_g is about 40°C higher than that of the free PTMO. In the three PTMO-2000 samples the T_g drops by 20°C to a value of about −60°C, indicating a marked improvement in phase segregation. The T_g also varies slightly, decreasing further with increasing hard-segment content. In the sample with the highest hard-segment content, PU2S34, the T_g is only about 10°C above that of free PTMO (−80°C), indicating that this sample is highly phase-separated. These suggestions regarding the extent of phase mixing are supported by the decrease in T_g of PU1S44 from −40 to −47°C with annealing but a change of only 1°C for PU2S34 on annealing. Note that PU2S68 shows soft-segment melting at 10°C, also consistent with a high degree of phase separation.

The heat capacity change ΔC_p (cal g^{-1} K^{-1}) was divided by the heat capacity change reported for ideal glassy PTMO[15], 0.195 cal g^{-1} K^{-1}, and by the weight fraction of soft segment to obtain values for the fraction of free soft segment listed in *Table 1*. The values decrease with increasing hard-segment content from a high of 0.58 to a low of 0.25. Although the values may seem surprisingly low, they are consistent with other data in the literature indicating extensive mixing with the hard-segment phase[11,15]. The values for the fraction of free soft segment, at comparable hard-segment content, are substantially higher in the PTMO-2000 than the PTMO-1000 series, in keeping with the superior phase separation indicated by the lower T_g in the higher-molecular-weight PTMO samples. These results indicate that a substantial fraction of the soft segment in all samples is incorporated in the hard-segment structure, either the interfacial region or possibly also within the organized portion of the hard-segment microdomains.

The scans over the high-temperature range show a distinct hard-segment T_g in the range 95 to 104°C in the PTMO-1000 samples (*Figure 2a*). In PTMO-2000 samples (*Figure 2b*) the behaviour is more complicated. The lowest hard-segment sample exhibits a classical glass transition, but with increasing hard-segment content the transition region takes on the character of a broad endotherm. Moreover, the transition temperatures are appreciably higher than the value of about 110°C for the hard-segment glass transition temperature. The transition appears to correspond to the T(1) endotherm described by Leung and Koberstein[10], representing a non-crystalline but not completely amorphous phase.

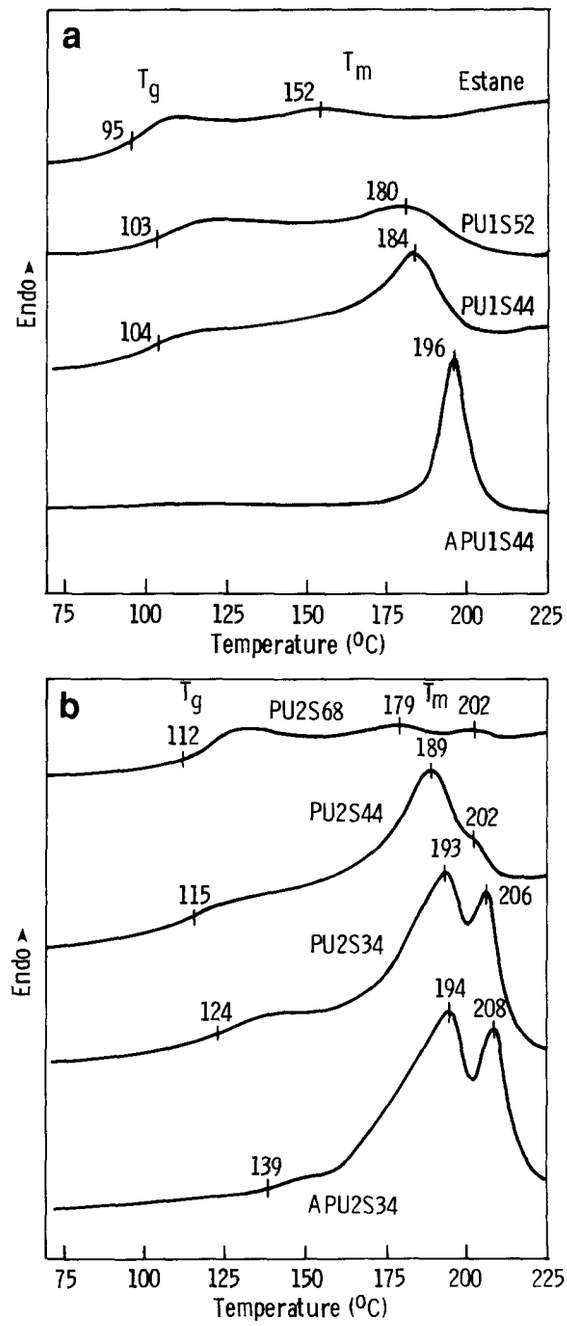

Figure 2 D.s.c. scans over the high-temperature range

This could have resulted from the prolonged 80°C annealing history associated with solvent removal, but this was not investigated.

The temperature and strength of the single hard-segment melting endotherm in the PTMO-1000 samples increases strongly with hard-segment content. In the PTMO-2000 samples there is a characteristic double peak. The endotherm occurring below 200°C is similar to that in the PTMO-1000 samples. The higher-temperature endotherm, which occurs above 200°C, is evident even in PU2S68, the sample with the smallest hard-segment content. This suggests that both a higher degree of hard-segment crystallinity and improved crystalline order occur in the hard-segment phase of the PTMO-2000 samples. Annealing has a marked effect on the temperature and sharpness of the melting peak in PU1S44, corresponding to the drop in soft-segment T_g. Annealed PU2S34 shows an increase in area for the melting endotherm but little increase in T_m. Annealing also removes or considerably diminishes the previously distinct hard-segment T_g. The estimated enthalpy change associated with the melting transitions is listed in *Table 1*. The values increase strongly with increasing hard-segment content. Following annealing, the enthalpy for PU2S34 is close to that for the pure MDI–BD copolymer.

Stress–strain measurements

Stress–strain measurements over a limited extension were carried out with the purpose of determining the initial modulus and the shape of the force–extension curve at low strain. The curves (*Figure 3*) show typical elastomeric behaviour, with a high initial slope, turning concave to the strain axis and continuing with a much smaller positive slope. For PU2S34, however, the sample exhibits yield behaviour and reaches the breaking point at relatively low elongation. There is also a sharp change in slope for PU2S44, suggestive of yield behaviour, but not in PU1S44. This difference, again, might be the result of the greater degree of phase segregation in the PTMO-2000 sample and the effect on the structure. The change in mechanical behaviour indicates a transition from isolated hard-segment microdomains to a bicontinuous structure or, possibly, a continuous hard-segment structure and isolated soft-segment regions, starting at about 56% hard segment in the PTMO-2000 samples. Previous electron microscopy studies on similar samples[5] have shown that a fibrous, open spherulitic structure can develop, which becomes more completely space-filling at higher hard-segment content. It is not clear whether the amorphous hard-segment structure is localized at phase boundaries or included within the crystalline phase. Modulus values are listed in *Table 2*, determined from the initial slope. It is clear that the modulus increases more rapidly than the hard-segment content. Also, there is a marked discontinuity in the modulus increase from PU2S68 to PU2S44 and PU2S34, in keeping with the appearance of the yield behaviour in the stress–strain curve.

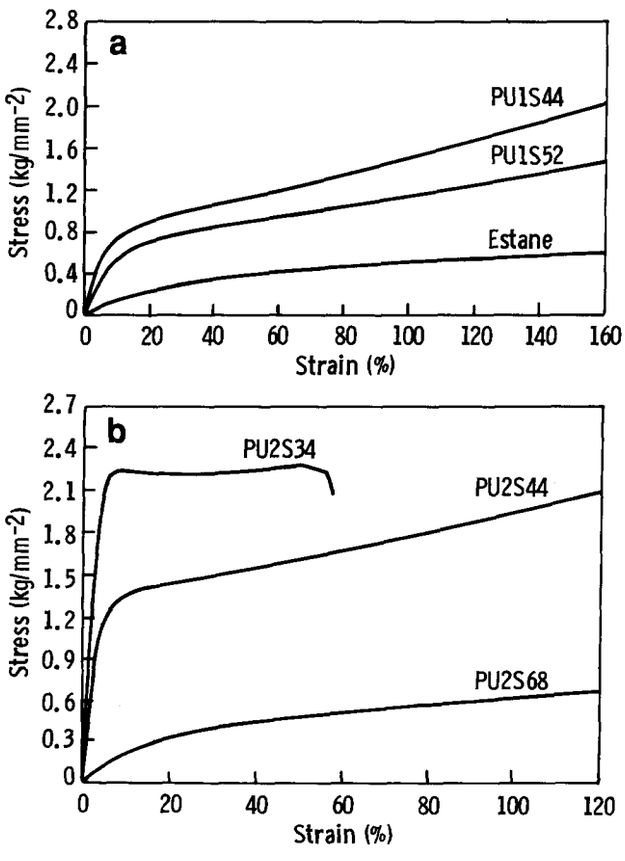

Figure 3 Stress–strain curves for various polyurethanes

DCE liquid solubilities

The values for DCE uptake under liquid immersion conditions are listed in *Table 2*. It is interesting that neither the Estane sample nor PU2S68 were soluble, despite the very high swelling levels, possibly due to the presence of a small degree of hard-segment crystallinity in these two samples. Measurements were also made on the DCE solubility in a partially crystalline MDI–BD copolymer and in the fully amorphous MDI–BD copolymer, which was based on the substitution of a branched diol for butanediol. On the basis of the relative DCE solubilities of 8% and 20%, respectively, a crude estimate of the crystallinity in the MDI–BD copolymer can be made, amounting to 60%. The percentage hard-segment crystallinity in the polyurethane samples can then be estimated from the melting enthalpies relative to that of MDI–BD (see *Table 1*). With this information, the DCE solubilities in *Table 2* can be corrected for the small contribution of solubility in the amorphous hard segment. There are then two possibilities to consider in comparing the DCE solubilities for the different samples. Sorption could be restricted to the fraction of free soft segment or could also occur in the soft-segment component included within the hard-segment structure. The swelling data, adjusted for these two possibilities, are compared in *Table 2*. The data, when normalized to the fraction of free soft segment, result in very high values. Moreover, these values do not decrease with increasing hard-segment content in response to the increased elastic constraints. The values for swelling, normalized to the total soft-segment content, appear to be more reasonable and follow the general trend expected with increasing hard-segment content. Thus, these results suggest that swelling involves almost all of the soft segment component.

In an ordinary crosslinked elastomer the swelling is inversely proportional to the elastic modulus. The product values of the DCE swelling, as weight per cent in the soft segment, and initial modulus are listed in the

Table 2 Tensile modulus E and DCE solubility in polyurethane samples

Sample	Modulus, E, (kg mm^{-2})	Wt DCE in PU (g/g)	Wt DCE in free SS (g/g)	Wt DCE in SS (g/g)	Wt% DCE in SS $\times E$
Estane	1.5	4.50	14.64	7.03	1054
PU1S52	6.0	1.10	5.87	1.94	1164
PU1S44	10.0	0.95	8.12	2.03	2030
PU2S68	2.5	2.60	6.43	3.73	932
PU2S44	35.0	1.00	5.28	2.06	7210
PU2S34	46.0	0.62	6.12	1.53	7038

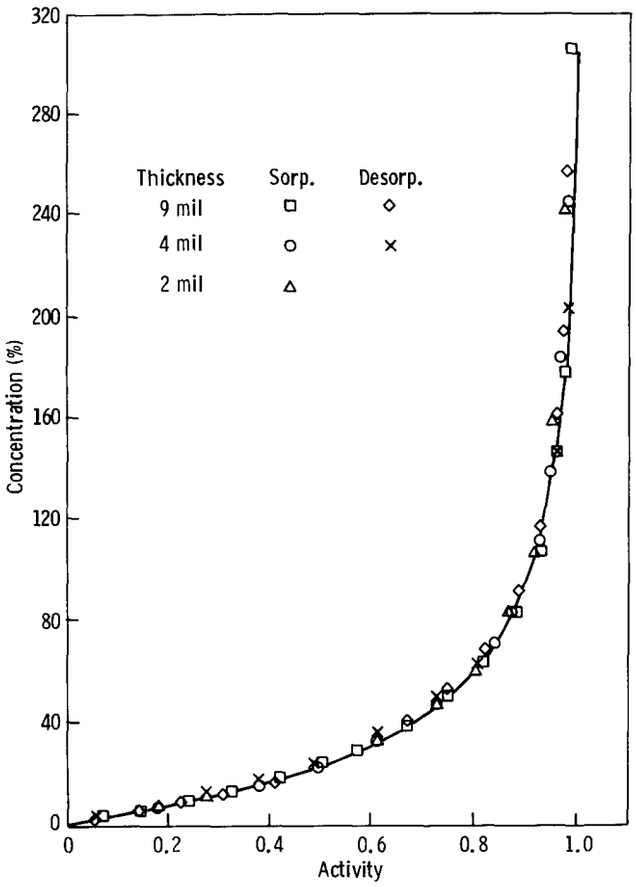

Figure 4 Sorption isotherm for Estane sample, showing results from sorption and desorption cycles for samples of three thicknesses

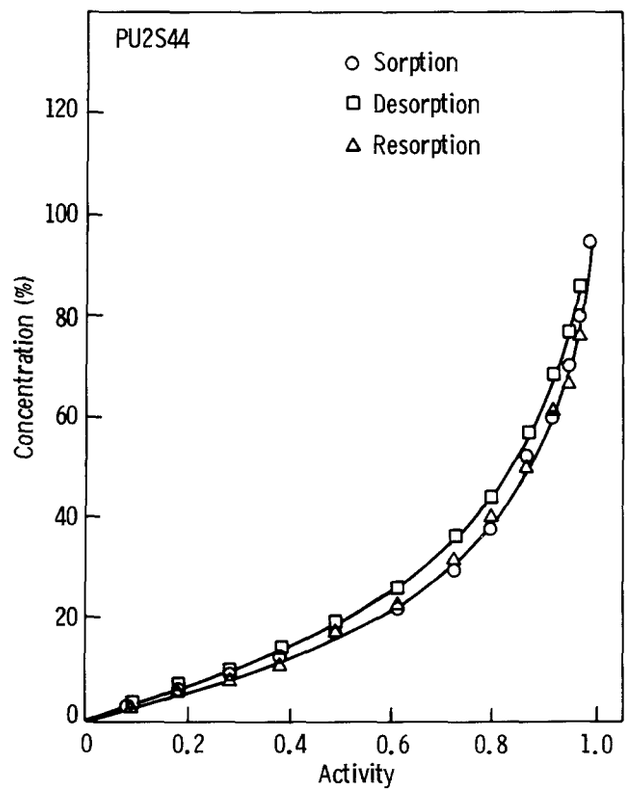

Figure 5 Sorption isotherm for PU2S44, showing results from sorption, desorption and resorption cycles

last column of *Table 2*. The values vary widely with hard-segment content and lead to exceptionally high product values for the higher hard-segment polyurethanes. This indicates that, unlike the crosslinked elastomer, the structural features that control the mechanical behaviour in the phase-segregated elastomer do not exert a comparable influence on the liquid swelling behaviour.

Sorption isotherms

The sorption data for the Estane sample at 24°C, representing DCE concentration ((grams solvent/gram polymer) × 100) against vapour activity (p/p_0), are shown in *Figure 4* for sorption and desorption runs on samples of three thicknesses (1 mil = 10^{-3} inch $\simeq$ 25 μm). All points fall on a single curve, which shows an initial linear region, then bends sharply upwards at higher activities in a manner typical of a strongly swelling solvent. The isotherm is, therefore, thickness-independent, as expected, and shows no hysteresis between the sorption and desorption cycles. If extrapolated to unit activity, the curve would be consistent with the immersion uptake of 450%.

The sorption isotherm for PU2S44 is shown in *Figure 5* for the initial sorption, desorption and repeat sorption cycles. In this case, the desorption curve is higher than the initial sorption and the repeat sorption curve falls in between but closer to the initial sorption curve. In general, similar mild sorption/desorption hysteresis was observed with all except the Estane sample, to a degree which increased somewhat with the hard-segment content. Apparently, the interaction of the solvent with the hard-segment or interphase regions during sorption results in some relaxation of the structure, which persists, in part, on the desorption cycle. Attempts to fit any of the isotherms with the Flory–Rehner relation[16] for the

swelling of a crosslinked elastomer were unsuccessful. Although a good fit could be obtained over the initial half or more of the activity range, the experimental curve rose more steeply than the predicted curve at higher concentrations. This might be expected if structural relaxation accompanies swelling.

Diffusion behaviour

A variety of vapour sorption and desorption rate curves were observed, depending on DCE concentration and sample type. Illustrations of the principal types of behaviour will be presented rather than a description of each sample. The vapour sorption and desorption rate curves for DCE in the Estane sample were Fickian[17] in appearance at low to moderate activities but showed sigmoidal behaviour above an activity of about 0.60. The sigmoidal behaviour became increasingly pronounced at higher activities. An example is shown for the 9 mil ($\simeq 230\ \mu m$) sample in *Figure 6*. It can also be seen that the slope of the sorption curves first increases and then decreases with increasing activity, indicating that the diffusion constant D goes through a maximum with concentration. Similar, but somewhat less pronounced, sigmoidal behaviour appeared in the sorption and desorption curves of PU2S68. This behaviour of DCE in the Estane sample differs from that of ODBZ, where distinct two-stage behaviour occurred in the sorption curves at moderate and high activities and where the desorption curves were Fickian in appearance.

The sigmoidal non-Fickian sorption and desorption behaviour of DCE occurred only in the two samples having the lowest hard-segment content. Two-stage sorption rate curves were observed in all the other samples above an activity of about 0.62. The severity of the two-stage behaviour generally increased with DCE concentration. However, the desorption curves remained Fickian in appearance at all activities. The two-stage character decreases with increasing sample thickness, as represented in *Figure 7* for PU1S44. This is the behaviour expected for sorption with a relaxation-controlled contribution. Repeat cycling decreases the severity of the two-stage character of the sorption curve, indicating some permanent change in structure following the initial DCE sorption cycle. However, as shown in *Figure 8*, the sorption curve lies below the desorption curve and retains some slight non-Fickian character in the nature of a slow approach to equilibrium.

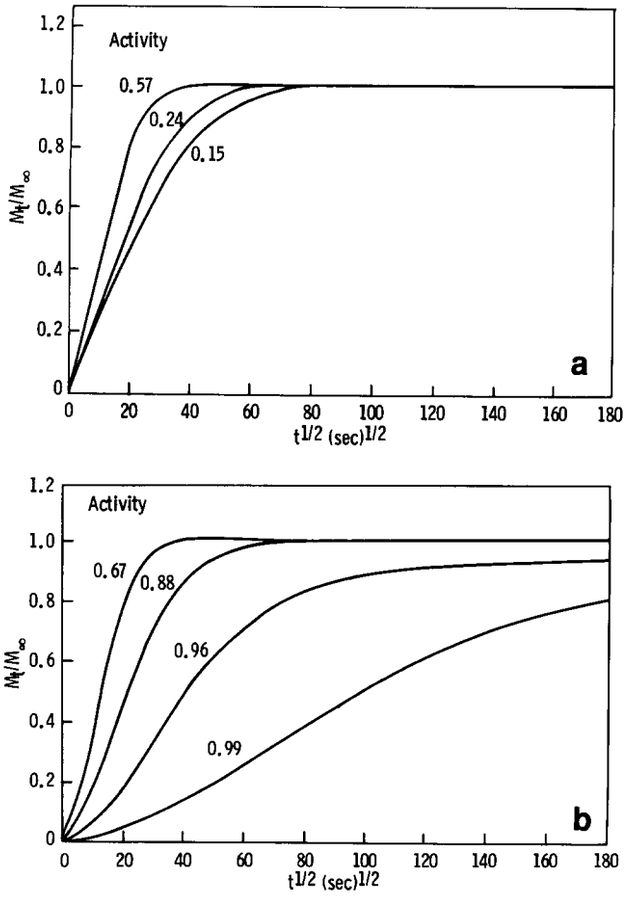

Figure 6 Sorption curves for Estane sample at various activities

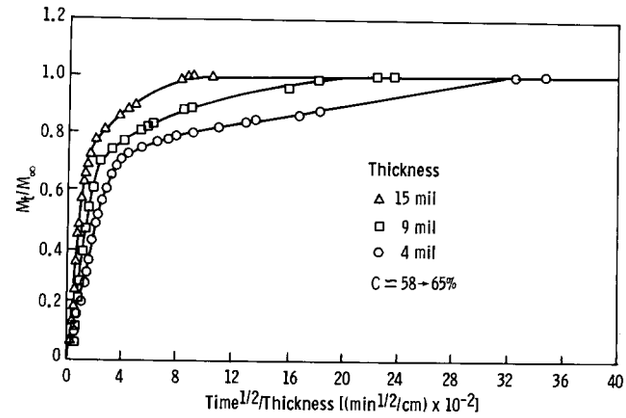

Figure 7 Sorption curves for PU1S44 at three thicknesses

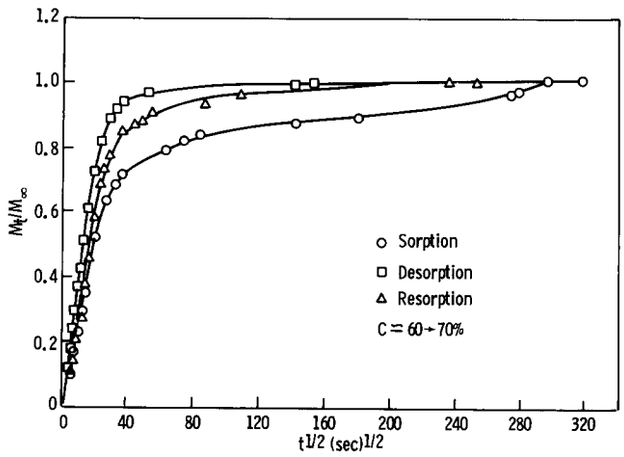

Figure 8 Sorption/desorption curves for PU2S44 showing effect of repeat cycling in a film of 9 mil thickness

Analysis of sorption curves

If diffusion obeys Fick's second law with requisite initial and boundary conditions[17], the fractional weight gain M_t/M_∞ will be a function solely of Dt/L^2, where M_t is the weight gain at time t, M_∞ is the equilibrium uptake and L is the thickness (cm). The curve of M_t/M_∞ plotted against the square root of time will go through the origin and will be linear over 60% of the initial uptake, then turn concave to the time axis and follow a monotonic approach to equilibrium. Furthermore, for samples

differing only in thickness, curves of M_t/M_∞ will superimpose when plotted as a function of the square root of reduced time, $(t/L^2)^{1/2}$. For Fickian sorption or desorption, D can be calculated from the initial slope:

$$D = \frac{\pi L^2}{16}\left[\frac{\mathrm{d}(M_t/M_\infty)}{\mathrm{d}t}\right] \quad (1)$$

or from the time $t_{1/2}$ to reach one-half sorption equilibrium:

$$D = 0.492L^2/t_{1/2} \quad (2)$$

It has been shown that the DCE sorption curves cover a range of behaviour, varying from Fickian to sigmoidal or two-stage, depending on conditions. This behaviour can be treated, phenomenologically, in terms of a suitable model of combined Fickian diffusion and relaxation processes developed by Joshi and Astarita (JA)[18]. These two processes are linked through a coupling constant, Φ:

$$\Phi^2 = \Theta_D/\Theta_R \quad (3)$$

The quantity $\Theta_D = L^2/4D$ is the characteristic time for diffusion and $\Theta_R = 1/k_R$ is a characteristic time for relaxation, with k_R a first-order relaxation rate constant. The fractional weight uptake is given by the following equation:

$$M_t/M_\infty = f_D - m\{f_{DR}(t) - (\tan\Phi/\Phi)[1 - \exp(-t\Phi^2/\Theta_D)]\} \quad (4)$$

where m is the fraction of uptake due to relaxation. The quantities f_D and f_{DR} are, respectively, the series solution to Fick's second law and a related series, which includes the coupling constant Φ. For $\Phi \gg 1$, the behaviour reduces to classical Fickian diffusion. For $\Phi \ll 1$, i.e. relaxation very slow compared to diffusion, the equation reduces to the sum of independent Fickian diffusion and a first-order relaxation process. This latter, simple model was initially proposed and widely used by Berens and Hopfenberg[13].

The quantities m, Φ and Θ_D were obtained from a least-squares fitting procedure applied to the experimental data. Examples of the fit, with resulting parameters, are shown in *Figure 9* for a sigmoidal DCE sorption curve and in *Figure 10* for two-stage sorption.

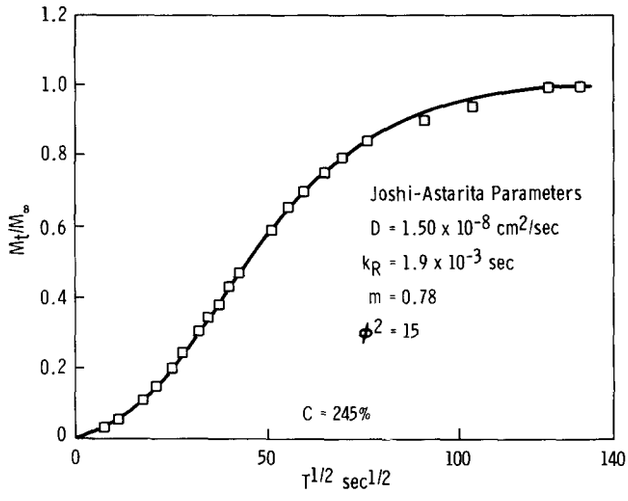

Figure 9 Joshi–Astarita fit to sigmoidal sorption curve for Estane sample, 9 mil thickness

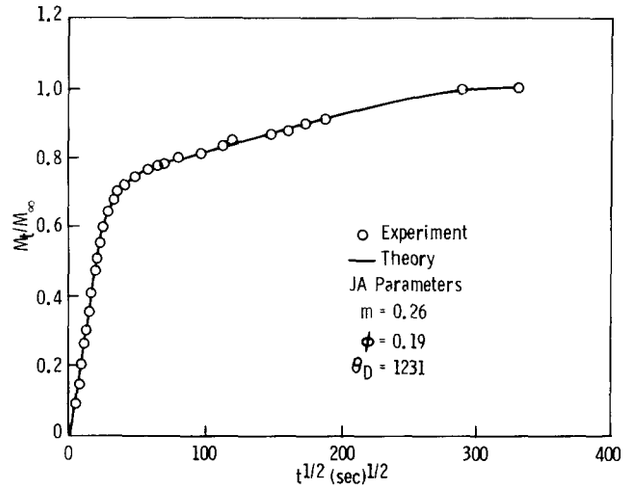

Figure 10 Joshi-Astarita fit to two-stage sorption curve for PU1S44, 9 mil thickness

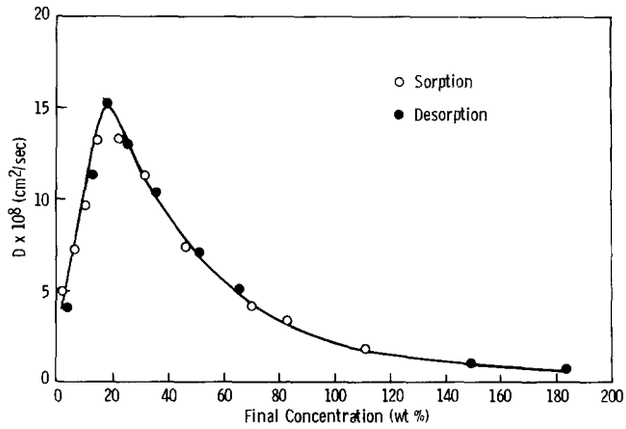

Figure 11 Concentration dependence of diffusion coefficient for Estane sample, 4 mil thickness, determined on the sorption and desorption cycles

The analysis provides a satisfactory fit to the data and yields values for the diffusion coefficient, the relaxation rate constant and the relative Fickian and relaxation contributions to the uptake. A sensitivity analysis has indicated that the diffusion coefficient can be determined with far greater accuracy than the other two parameters. Since this is also the parameter of greatest interest, only the diffusion results will be treated in detail. However, it is worth while summarizing the trends in the other parameters. In the data for the 9 mil Estane film, the value of m increased from about 0.3 to 0.8 with increasing concentration; Φ increased from about 2 to 8; and k_R remained fairly constant at 1×10^{-2} up to a concentration of 84% and then decreased rapidly to a final value of 0.1×10^{-2} at 306% concentration.

The resulting concentration dependence of the diffusion coefficient, shown in *Figure 11* for the Estane sample, goes through a pronounced maximum and the results from sorption and from desorption nearly coincide. This contrasts with the behaviour reported with ODBZ, where the desorption results were higher than those from the sorption cycle. For PU2S44, which showed two-stage sorption and Fickian desorption, there is, nonetheless, close correspondence between the diffusion results for the sorption, desorption and repeat sorption cycles. The general agreement between the sorption and desorption

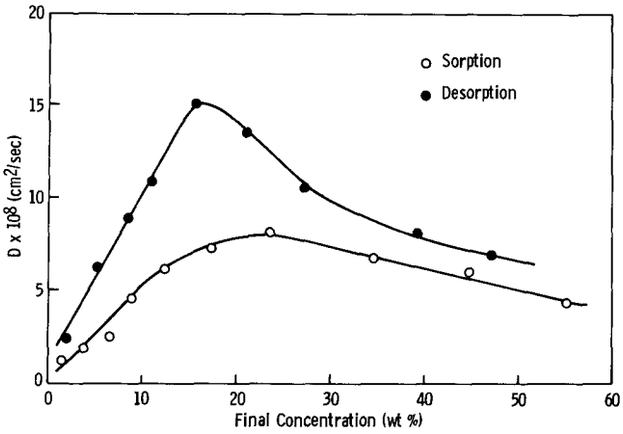

Figure 12 Concentration dependence of the diffusion coefficient for PU2S34 sample, 4 mil thickness, determined on the sorption and desorption cycles

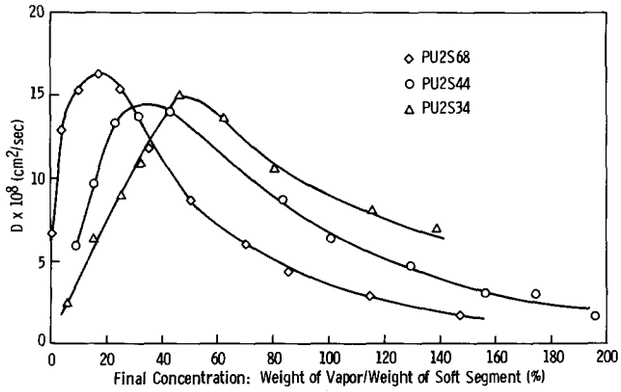

Figure 13 Comparison of *D versus C* curves from desorption runs on three PTMO-2000 samples, with concentration as weight vapour/weight soft segment. All samples 4 mil thickness

results indicates that the diffusion coefficients obtained from the JA analysis are physically realistic. For almost all other samples, there was comparable agreement for the diffusion constants from sorption and desorption runs. The exception was PU2S34, the sample with the highest hard-segment content. In this case, the desorption results were distinctly higher than the results from the sorption runs, as shown in *Figure 12*.

A comparison of the *D versus C* curves for the three samples with 2000 molecular-weight soft segment against the concentration of sorbed vapour, normalized to the soft-segment content in each sample, is shown in *Figure 13*. These curves, although similar in appearance, show that *D* is lower for the higher hard-segment samples below the maximum in *D versus C*. However, the trend reverses above the maximum where *D* becomes higher for the higher hard-segment samples. Any attempt to interpret this behaviour in structural terms must await the analysis of a later section.

Thickness dependence of the diffusion coefficient

Sorption experiments were run as a function of thickness on two types of samples: the Estane sample, which showed sigmoidal sorption and desorption curves above a concentration of about 35%, and PU1S44, which showed two-stage sorption behaviour at concentrations exceeding 25%, but overall Fickian desorption. The *D versus C* curves for the Estane samples, for sorption runs at three thicknesses, are shown in *Figure 14*. There is a pronounced increase in the diffusion data with thickness, amounting to a factor of 6 for the maximum diffusion coefficient from the 2 to the 9 mil samples. If the JA model is applicable, the resulting values of *D* should be independent of thickness. However, similar thickness-dependent results were obtained for PU1S44 from desorption runs on samples of 4, 9 and 15 mil thickness (*Figure 15*). In this case, the desorption runs are Fickian and, therefore, the values of *D* were obtained directly from the half-time. This indicates that the thickness dependence has a more fundamental origin than any limitation of the JA treatment.

It was realized in work carried out with toluene in natural rubber[19] that significant heating effects might accompany vapour sorption and desorption. Such heating effects are well known for the sorption of water in wool and organic polymers, and the analysis has been carried out by Armstrong and Stannett[20,21], which permits the correction of the measured diffusion coefficients. The occurrence of heating effects with toluene in

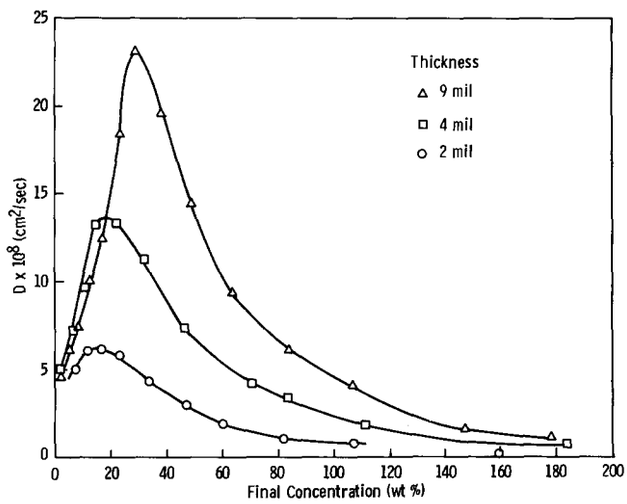

Figure 14 Comparison of *D versus C* for Estane at three thicknesses from sorption runs

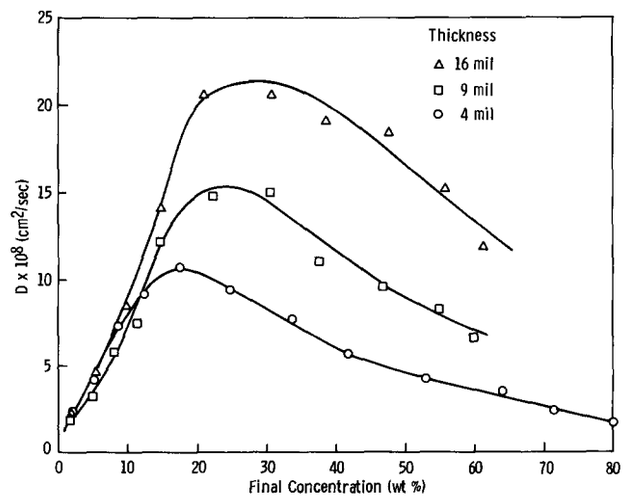

Figure 15 Comparison of *D versus C* curves for PU1S44 for three thicknesses from desorption runs

natural rubber, despite the low heat of vaporization relative to that of water, is due to the high temperature coefficient of weight gain at constant pressure, ω, which occurs in highly swelling liquids. In the absence of measurements of the temperature coefficient of regain, an estimate of ω can be obtained from the slope of the sorption isotherm:

$$\omega = \frac{1}{\Phi_2^2}\left(\frac{H_v}{RT^2}\right)\left(\frac{\partial \Phi_1}{\partial \ln a}\right)_{T,p} \quad (5)$$

The derivation of this relation will be given in a future publication. The other quantities required in applying the Armstrong–Stannett analysis are: the heat of vaporization of DCE, 7429 cal g^{-1} mol^{-1}; the heat capacity of the polymer, taken as 0.3 cal g^{-1} $°C^{-1}$; the final slope of the sorption rate curve, plotted as $\ln(1 - M_t/M_\infty)$ *versus* t, which was approximated from the value of D as $\pi^2 D/L^2$ (ref. 17). In addition a value for the heat transfer coefficient is needed. A value of 3.0×10^{-4} cal cm^{-2} s^{-1} was used. This is twice the value determined by Armstrong and Stannett. It might be justified by a higher contribution of convection, due to the relatively high DCE vapour pressures compared to water, in the range of activities examined by those authors, as well as the five-fold higher density of the vapour at a given activity, due to the higher molecular weight of DCE. The result of this analysis applied to DCE in the Estane sample, at a concentration of about 110%, was an increase in D by a factor of about 2 for all three thicknesses. This shows that heating effects must be taken into account if the magnitude of the diffusion coefficient is important. However, the calculations also indicate that the heating effects cannot account for the thickness dependence of the diffusion coefficient.

Conversion to solvent mobilities

The conversion of the diffusion results to solvent mobilities D_1 is helpful in pursuing a physical interpretation of the D *versus* C behaviour. Since the solvent mobilities should follow free-volume theory as a function of concentration and reach a limiting value equal to the self-diffusion coefficient of the pure solvent D_1^*, this also provides a test of the reliability of the diffusion results. The diffusion constant obtained in a sorption experiment can be related to the product of the solvent mobility D_1 and a thermodynamic factor Q (ref. 22):

$$D = D_1 Q \quad (6)$$

where Q expresses the thermodynamic driving force for diffusion, $\mathrm{d} \ln a_1 / \mathrm{d} \ln \Phi_1$. Since D_1 will generally increase with concentration and Q decreases with concentration, depending on the relative rate of change, D will go through a maximum when the measurements are carried out over a sufficiently large concentration range.

The diffusion coefficient obtained in incremental sorption, using equation (1) with the dry sample thickness L, approximates a mean diffusion coefficient $\bar{D}(C)$ in the sorption interval. It was shown by Duda *et al.*[23] that the actual diffusion coefficient $D(C)$ can be set equal to $\bar{D}(C)$ for some prescribed C in the interval. The position depends only on whether D increases or decreases with C. In order to proceed to the solvent mobility, it is then necessary to convert $D(C)$ to the mutual coefficient D_{12} by applying the relation derived by Crank[17]:

$$D_{12} = D/\Phi_2^2 \quad (7)$$

The solvent mobility is obtained using the semiempirical relation[24]:

$$D_{12} = D_1 \Phi_2 (\partial \ln a_1 / \partial \ln \Phi_1)_{T,p} \quad (8)$$

where all terms in this relation are defined for the same concentrations that apply in calculating $D(C)$. The assumptions underlying this equation have been discussed critically by Duda *et al.*[24], who also verified the relation experimentally for one polymer–solvent system.

The preceding relations were applied to sorption data for the 9 mil Estane film. For simplicity, the microdomains were treated as inert filler and the solvent concentration adjusted for the volume of the soft-segment phase. The required values of the thermodynamic correction factor were obtained by graphical differentiation of the sorption isotherm. The resulting values of the solvent mobility are plotted in *Figure 16* against the solvent volume fraction. The solvent mobility increases monotonically with concentration and can be extrapolated to a value of about 3.7×10^{-6} cm^2 s^{-1}. This is a factor of about 10 lower than an estimated value of the self-diffusion coefficient D_1^* for the pure liquid DCE, based on a value of 3×10^{-5} cm^2 s^{-1} for benzene[25]. These results are in marked contrast to the behaviour of ODBZ in this same Estane sample, where D_1 levelled off at a value that was about 100-fold lower than the estimated self-diffusion coefficient for this liquid. If the corrections for the heating effect on the diffusion coefficient at a concentration of 110% are applicable to the extrapolated value, this would increase D_1 for DCE by a factor of 2. This is remarkably close to the estimated value of D_1^*. The value would be expected to increase further if an appropriate correction for the effect of the hard-segment structure were applied.

The preceding analysis is helpful in attempting to interpret the puzzling behaviour of the D *versus* C curves of the three PTMO-2000 samples (*Figure 13*). The extrapolation of these curves to zero concentration indicates that the zero-concentration diffusion coefficient D_0 properly reflects the hard-segment content, increasing in the order PU2S34, PU2S44, PU2S68. A somewhat more quantitative estimate of D_0, obtained from diffusion measurements with a poor solvent, n-heptane, indicated values of 1.5×10^{-8}, 3.0×10^{-8} and 4.5×10^{-8} cm^2 s^{-1}, respectively. The separation of the D *versus* C curves should reflect these relative D_0 values.

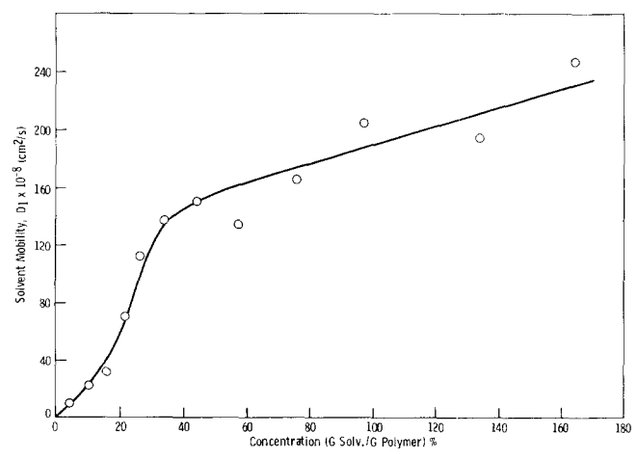

Figure 16 Solvent mobilities for 9 mil Estane sample *versus* volume fraction of soft segment, Φ_1

Table 3 Comparison of D, D' and D_1 at DCE volume fraction in the soft segment, $\Phi_1 = 0.5$

Sample	C (g DCE/g PU)	$D \times 10^8$ ($cm^2\ s^{-1}$)[a]	Ratio	$D' \times 10^8$ ($cm^2\ s^{-1}$)[b]	$D_1 \times 10^6$ ($cm^2\ s^{-1}$)[c]	Ratio
PU2S68	0.80	3.67	1.00	8.02	1.67	1.00
PU2S44	0.52	5.34	1.46	7.44	1.54	0.922
PU2S34	0.44	7.55	2.05	10.90	2.95	1.77

[a] D, obtained from the analysis of desorption data
[b] D', corrected for heating effects
[c] D_1, solvent mobilities following correction for heating effects

At low concentrations the slope of the D *versus* C curves increases in the order of increasing soft-segment concentration, as would be expected from the restrictions imposed by the hard-segment structure. A possible cause of the reversal in order above the maximum is the effect of the thermodynamic correction factor, which could be larger for the sample of lowest soft-segment content. This can be tested by conversion to solvent mobilities, which removes the contribution of the thermodynamic factor. However, before conversion to solvent mobilities can be applied, the possible role of heating effects must be examined. The data are summarized in *Table 3* for a DCE volume fraction in the soft-segment phase of all samples equal to 0.5. This corresponds to the various solvent concentrations listed in the second column as weight of DCE per unit weight of polymer. The table compares the original values D with the results D' obtained following corrections for the heating effect and with the solvent mobilities D_1. The effect of the heating corrections is to narrow the differences significantly. However, the D_1 value for the highest hard-segment sample is almost twice the value of the other two samples and fully half the value of the heat-corrected D_1 for the Estane sample at $\Phi_1 = 0.5$. By comparison with the trend in the D_0 values, the D_1 results are unusually high for PU2S44 and PU2S34 relative to PU2S68.

One possible explanation for these unexpectedly high values of the diffusion coefficient for the higher hard-segment samples is a solvent-induced change in structure that facilitates diffusion. Sample PU2S34 showed significant hysteresis in the sorption isotherm. In addition, there was a marked increase in D on the desorption compared to the sorption cycle (see *Figure 12*). These observations are indicative of a solvent-induced structural change. Solvent-induced relaxation could also account for the extremely high relative values recorded in *Table 2* for the product of the DCE solubility and the initial modulus for the two higher hard-segment samples.

It is possible to provide a qualitative model that could account for the various observations. The parallel packing and crystalline order in hard-segment microdomains and limited lamellar thickness require chain folding of the MDI–BD units. As a result, the disordered interfacial region represents a large fraction of the hard-segment structure. The mixing of the soft-segment with the hard-segment structure probably occurs primarily in the interfacial region. If this assumption is correct, it is easy to understand why almost all of the soft segment is accessible to the solvent, as suggested by the results of *Table 2*. It is not necessary to postulate extensive swelling of the organized hard-segment structure or even swelling of any possible included soft-segment component. The extreme swelling stress generated in the interfacial region would give rise to microfracture in blocks of hard-segment structure. This would increase the overall sorption level and reduce the impedance to diffusion.

CONCLUSIONS

The sorption and diffusion of a highly swelling liquid in a phase-segregated polymer is a complicated process. At low solvent concentrations diffusion is nominally Fickian. However, at higher concentrations anomalous diffusion curves varying from sigmoidal to two-stage are obtained, which are evidence of solvent-induced structural change in the hard-segment microdomains or in the interfacial region. These curves can be analysed phenomenologically in terms of the Joshi–Astarita model of coupled Fickian diffusion and a first-order relaxation process.

The diffusion coefficient *versus* concentration curves for all samples show a maximum, indicating the importance of the thermodynamic correction factor in determining the concentration dependence. A detailed analysis of the results for the 9 mil Estane sample was carried out to determine the behaviour of the solvent mobilities. In this case, the resulting values approached within an order of magnitude of the estimated self-diffusion coefficient of pure DCE. The values would be increased further by corrections for the predicted heating effects accompanying sorption and the influence of the hard-segment structure as an obstacle to diffusion and as a physical crosslink network. It also appears that solvent swelling can induce structural changes in the higher hard-segment polyurethanes, leading to higher than expected values for the liquid solubility and for the diffusion coefficient at high concentrations. It must be admitted that the exact nature of these changes or of the process referred to as relaxation is not known but might be clarified by details of the emerging model of the structure of MDI-based polyurethanes.

It is interesting to compare the two solvents, DCE and ODBZ, in their effect on the Estane sample. With ODBZ the sorption curves were two-stage and desorption curves were Fickian, whereas with DCE the curves on both cycles were sigmoidal. The two-stage behaviour corresponds to smaller values of the coupling constant Φ, implying slower relaxation compared to diffusion. This, together with various other comparisons cited in the earlier discussion, indicates that DCE is more effective in promoting relaxation and mobility in the hard-segment structure or interfacial regions. Perhaps, studies employing other solvents to examine possible solvent-specific differences would be helpful in understanding the processes that accompany sorption and diffusion in these materials.

It has been shown that the Joshi–Astarita analysis of combined diffusion and relaxation provides a useful phenomenological model for fitting the various non-Fickian sorption rate curves in order to obtain values of the diffusion coefficient. However, a disturbing result, which follows from the analysis of the Estane sorption rate curves, is the strong thickness dependence in the derived diffusion data. The diffusion data obtained from the desorption rate curves of PU2S34, which are Fickian, also exhibit a strong thickness dependence. In both cases, the data increase with thickness, in keeping with the behaviour expected for a relaxation-controlled process. In the phase-segregated polyurethanes, sorption is probably controlled by relaxation of the hard-segment structure, as proposed in an earlier study[12]. It is not clear whether an appropriate model for this process could explain the results obtained here. At present there is no model which indicates that it is possible to have relaxation-controlled sorption and still have Fickian-appearing sorption curves. Therefore, a general question to be answered is whether it is possible to have some type of relaxation effect, leading to thickness dependence of D, and still have Fickian-appearing sorption curves or whether there must be some other cause of the anomalous behaviour.

REFERENCES

1 Seymour, R. W. and Cooper, S. L. *Rubber Chem. Tech.* 1974, **47**, 19
2 Hesketh, T. R., Van Bogart, J. W. C. and Cooper, S. L. *Polym. Eng. Sci.* 1980, **20**, 190
3 Van Bogart, J. W. C., Bluemke, D. A. and Cooper, S. L. *Polymer* 1981, **22**, 1428
4 Zdrahala, R. J., Critchfield, F. E., Gerkin, R. M. and Hager, S. L. *J. Elastomers Plast.* 1980, **12**, 194
5 Schneider, N. S., Desper, C. R., Illinger, J. L., King, A. O. and Barr, D. *J. Macromol. Sci.-Phys.* 1975, **B11**, 527
6 Abouzahr, S., Wilkes, G. L. and Ophir, Z. *Polymer* 1982, **23**, 1977
7 Miller, J. A., Lin, S. B., Hwang, K. K. S., Wu, K. S., Gibson, P. E. and Cooper, S. L. *Macromolecules* 1985, **18**, 32
8 Blackwell, J., Chivers, R. A., Gutierrez, G. A. and Biswas, A. *J. Macromol. Sci.-Phys.* 1985, **B24**, 39
9 Briber, R. M. and Thomas, E. L. *J. Polym. Sci., Polym. Phys. Edn* 1985, **23**, 1915
10 Leung, L. M. and Koberstein, J. T. *J. Polym. Sci., Polym. Phys. Edn* 1982, **23**, 1060
11 Leung, L. M. and Koberstein, J. T. *Macromolecules* 1986, **19**, 706
12 Schneider, N. S., Mee, C. F., Goydan, R. and Angelopoulos, A. P. *J. Polym. Sci., Polym. Phys. Edn* 1989, **27**, 939
13 Berens, A. R. and Hopfenberg, H. B. *J. Polym. Sci., Polym. Phys. Edn* 1979, **17**, 1757
14 Schneider, N. S. and Sung, C. S. P. *Polym. Eng. Sci.* 1984, **17**, 1835
15 Camberlin, Y. and Pascault, J. P. *J. Polym. Sci., Polym. Phys. Edn* 1983, **21**, 415
16 Flory, P. J. 'Principles of Polymer Chemistry', Cornell University, Ithaca, New York, 1953
17 Crank, J. 'Mathematics of Diffusion', 2nd Edn, Clarendon, Oxford, 1975
18 Joshi, S. and Astarita, B. *Polymer* 1979, **20**, 455
19 Waksman, L. S., Schneider, N. S. and Sung, N. H. in 'Barrier Polymers and Barrier Structures' (Ed. W. J. Koros), *ACS Symp. Ser.* in press
20 Armstrong, A. A. Jr and Stannett, V. *Macromol. Chem.* 1966, **90**, 145
21 Armstrong, A. A. Jr, Wellons, J. D. and Stannett, V. *Makromol. Chem.* 1966, **95**, 78
22 Vrentas, J. S. and Duda, J. L. *AIChE J.* 1979, **25**, 1
23 Duda, J. L., Ni, Y. C. and Vrentas, J. S. *J. Polym. Sci., Polym. Phys. Edn* 1977, **15**, 2039
24 Duda, J. L., Ni, Y. C. and Vrentas, J. S. *Macromolecules* 1979, **12**, 459
25 Rimschussel, W. and Hawlicka, E. *J. Phys. Chem.* 1974, **78**, 230